

# Ultra Low Velocity Ejecta Generated by Slow Impacts on Rubble Pile Asteroids

K. Joeris, L. Schönau, M. Keulen, and J.E. Kollmer

*University of Duisburg-Essen, Faculty of Physics, Lotharstr. 1, 47057 Duisburg, Germany*

(The author to whom correspondence may be addressed: kolja.joeris@uni-due.de)

(Dated: May 2024)

We examine ejecta generated by ultra low velocity impacts under asteroid conditions. In an environment of precisely controlled milligravity and under vacuum, impacts with velocities in the range of centimeters/second are performed with irregularly shaped impactors onto granular beds. The resulting ejecta velocities are compared to existing literature values and extend the observed systematic trends towards lower impact energies, broadening the parameter range. Simulations are performed to reason the systematics and the absence thereof for measurements performed at earth gravity. We find, that the cutoff induced by gravity dependent minimal observable velocities plays a crucial role in the values obtained for mean ejecta velocities.

## I. INTRODUCTION

Impact processes on celestial bodies have been studied experimentally and numerically extensively, but came into focus even more in the light of recent asteroid missions. Those missions delivered detailed images from asteroid surfaces, fueling research to understand formation and evolution of those objects. More than that, some even performed touchdown maneuvers<sup>1</sup>, sample returns<sup>2</sup> and impact experiments<sup>3</sup>. While those missions are extremely insightful concerning for example ejecta generation<sup>4</sup> and momentum transfer<sup>5</sup>, they come with an exceptionally high prize tag and low repetition rate. As a consequence, the main source for experimental data are ground based experiments<sup>6-9</sup>, backed by simulations<sup>10</sup>. Our experiments are focused on impacts into weakly bound granular surfaces, with the setup's aim to recreate the dynamics found on rubble pile asteroids<sup>11-13</sup>. With a surface gravity in the range of few  $\text{mm/s}^2$  or lower, the differences to granular dynamics on earth cannot be neglected. First, escape velocities will be small on those bodies<sup>14</sup>. As a result, ejecta generated by (fast) impacts will only re-impact the asteroid, if their ejection velocity is small as well, ranging in the  $\text{cm/s}$  regime. This filtering effect determines our focus on low velocity interactions. For those slow impacts under asteroid gravity, the force balance changes from what we observe in an environment with earth gravity<sup>15</sup>. With low gravity and low kinetic energy, the cohesive forces gain importance even for larger particle sizes. With the the increased contribution of cohesive forces, we cannot expect that scaling models that have been derived for higher energies will be readily generalizable to work on extremely weak gravitating rubble pile asteroids. Our analysis thus aims to extend the understanding of granular dynamics into this low energy, high cohesion regime. Granular matter in low gravity is extremely prone to experimental disturbances by even small forces and vibration, thus difficult to explore. While we already studied impactor rebound and regolith surface elasticity in an experiment that created an asteroid environment<sup>16</sup>, we now focus on the ejecta velocity distribution. Both topics are interconnected however, as the ejecta's velocity determines its trajectory and possible subsequent impact events.

To investigate the ejecta velocities, we performed low gravity impact experiments as well as DEM simulations that include inter particle cohesion. We then compare the ejecta velocities obtained in experiment and simulation to literature values<sup>8</sup>. The experiments were performed at the ZARM (Zentrum für angewandte Raumfahrttechnik und Mikrogravitation) Bremen drop tower. Defined asteroid gravity was created by a linear stage performing a constant acceleration to the sample chamber while the stage with the attached chamber were in free fall. This "linear stage in drop capsule" approach enables us to realize an environment of controlled asteroid gravity  $a_a = 2 \cdot 10^{-3} \text{ m/s}^2$ . With a vacuum chamber surrounding the experiment volume, the asteroid simulation is completed. Inside of this volume, a granular bed - mimicking the asteroids regolith covered surface - is located. During an experiment an impactor is launched onto the granular bed, while being observed by multiple cameras. See Fig. 1 for (a) the main cameras point of view, (b) particle tracks and (c) numerical simulation. For further details on the experiment and details on the DEM simulation, see the Methods section IV and the dedicated publication<sup>17</sup>.

## II. RESULTS

As an Overview, Fig. 2 presents all data of low velocity ejecta generation available to us. Shown here are the ejecta velocities  $v_e$  for different impactor velocities while neglecting all other parameters like bed particle size and impactor size. As this is a logarithmically scaled plot with respect to ejecta velocities, points with a value of  $v_e = 0$  cannot be consistently displayed. Just for this plot, impacts which create no measurable ejecta are not omitted but assigned a velocity of  $v_e = 0.1 \text{ cm/s}$ , making them clearly distinguishable from data points with visible ejecta. As a source for literature values of comparable experiments, we rely on values published by Brisset et al<sup>8</sup> shown in red. The Brisset data points are compiled from different experiments, including parabolic flights, space shuttle flights and a unique laboratory drop tower<sup>7,8,18,19</sup>.

For our data points, we have included both microgravity based experiments recreating asteroid environments (we forth

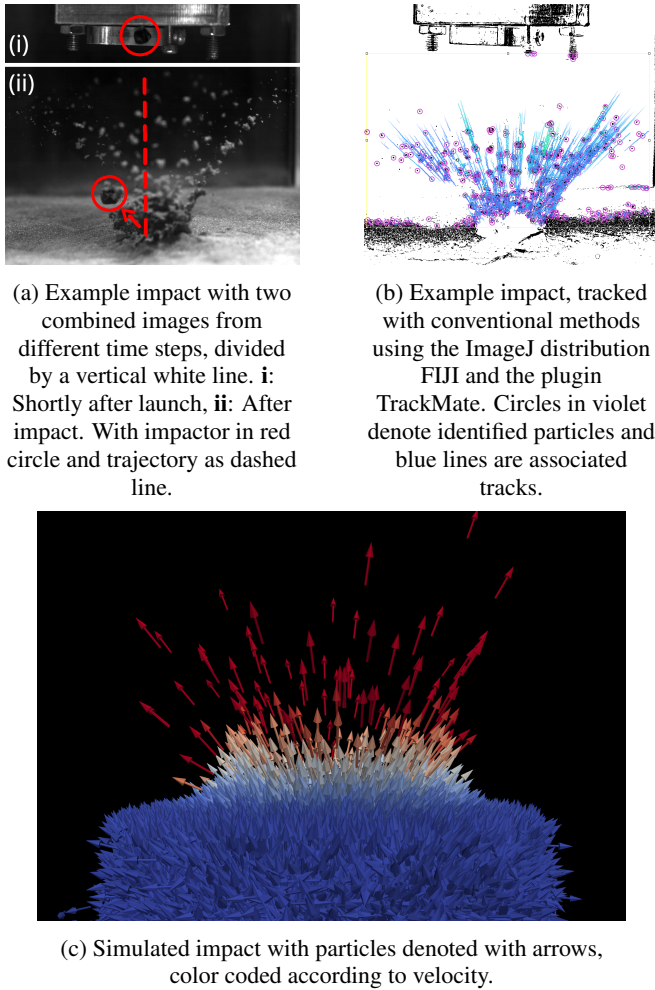


FIG. 1: Example ejecta plumes. Views from the main camera (a,b), one with two different time points and one with tracks and simulations (c).

call milligravity data) and earth gravity control experiments. Our data points are shown in blue for impacts under earth gravity and black for asteroid gravity in Fig. 2. While it seems reasonable to fit a linear function to our milligravity data, all other points spread wildly in this graph. There is no obvious systematic connection between the literature values and our data points. However, the picture changes completely when introducing a scaling similar to Brisset et al.<sup>8</sup>, by taking into account the ratio of impactor size  $D_p$  and the bed particle size  $d_g$  and the square root of the impactor's velocity. What follows from that for all of our data points combined with those from<sup>8</sup> is shown in Fig. 3. The values taken at earth gravity, plotted in blue, separate more clearly from our (black) and literature (red) microgravity values. On the other hand, when excluding earth gravity values, a much clearer trend emerges, as shown in Fig. 3. Our data for ultra low impactor velocities extend the point cloud of ejecta velocities towards lower energies. A linear fit matches the combined set of data points closely, verifying Brisset's semi-empirical law for an extended parameter range.

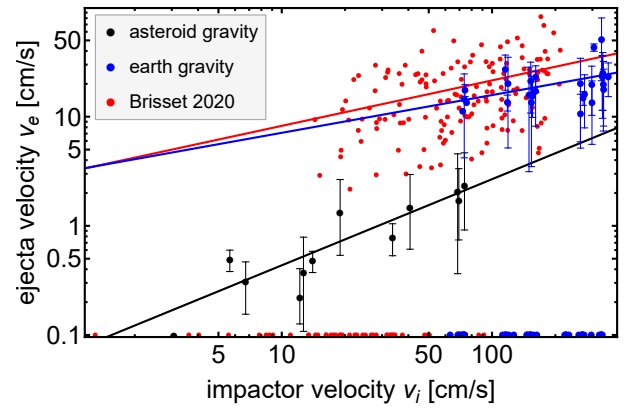


FIG. 2: All data points for ejecta velocities from literature<sup>8</sup> partial gravity experiments (red), our asteroid gravity  $a_a = 2 \cdot 10^{-3} \text{ m/s}^2$  experiments (black) and our earth gravity experiments (blue).

It is obvious from Fig. 3, that the data points we obtained from microgravity experiments align approximately with the literature values while extending it towards lower impactor energies. A change in the ejecta velocity behavior might be expected for low impactor energies under asteroid gravity, because cohesion becomes increasingly important for granular dynamics as shown in<sup>16</sup>. Still, we see no indisputable sign that we have entered this regime just by looking at ejecta velocities. This scaling on the other hand breaks when taking into account our data obtained under earth gravity (blue). No reasonable linear fit can be conducted here, with a low R-Squared of 0.0924 for the best fit. To investigate the reason for this discrepancy between gravity levels we use the DEM simulation. In contrast to the experiment, the DEM simulation gives us access to the full ejecta velocity distribution, see Fig. 5. The bold black dots in Fig. 5 denote the velocity distribution without cutoff. The black dots following a line in this double logarithmic plot indicates that the velocity distribution follows a power law. The small red dots in Fig. 5 are the velocities of a sub-selection of particles, notably those particles that travel above the original bed height. We chose this selection to create a velocity distribution only from particles that would be observable as ejecta in an experiment, in contrast to particles just wiggling around in the bulk regolith below the surface.

The simulations result with the ejecta only cutoff applied is shown in Fig. 4, displaying the ejecta velocities with the abscissa scaled in the same style as in Fig. 3. Six different gravity regimes are covered from asteroid gravity  $a_a = 2 \cdot 10^{-3} \text{ m/s}^2$  to earth gravity  $a_e = 10^4 \text{ m/s}^2$ . The distributions are evaluated at a time point, where the ejecta plume has fully formed. This time is gravity dependent and determined from the initial velocity a particle would need under the given environmental acceleration to reach a height of its own diameter, i.e. be observably displaced. The observation time  $t_o = \sqrt{d/a}$  with diameter  $d$  and acceleration  $a$  is determined from that by dividing the particle radius by this velocity. As seen in Fig. 4, ejecta velocities in the reduced gravity regimes exhibit a linear behavior for each gravity regime. But like in the ex-

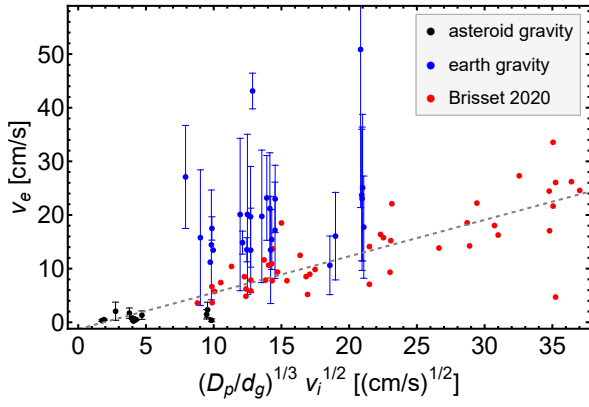


FIG. 3: Experimental ejecta velocities  $v_e$  with scaled abscissa. Blue Points: Our data in earth gravity. Black points: Our data in asteroid gravity. Red Points: Data collected by Brisset *et al*<sup>8</sup>. Dashed gray line: Linear fit to combined asteroid gravity data from both experimental sources.

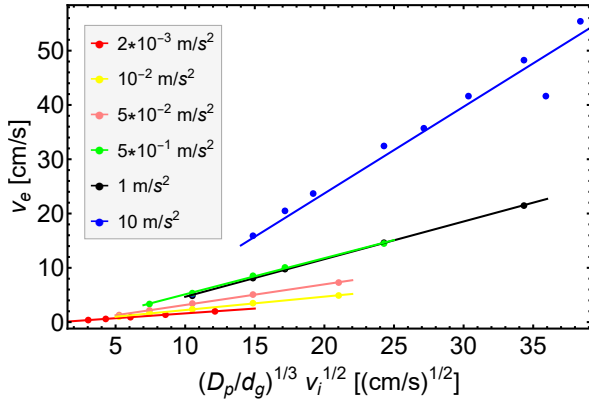


FIG. 4: Ejecta velocities taken from numerical simulations  $v_e$  with scaled abscissa. Six different accelerations from  $2 \cdot 10^{-3} \text{ m/s}^2$  to  $10 \text{ m/s}^2$  with linear models fitted.

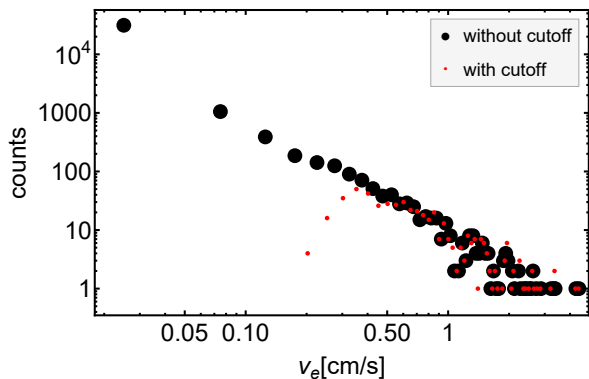


FIG. 5: Velocity distribution of ejecta from Simulation, binning with  $0.05 \text{ m/s}$ . Black: All velocities including granular bed. Red: Ejecta velocities with standard cutoff enforced.

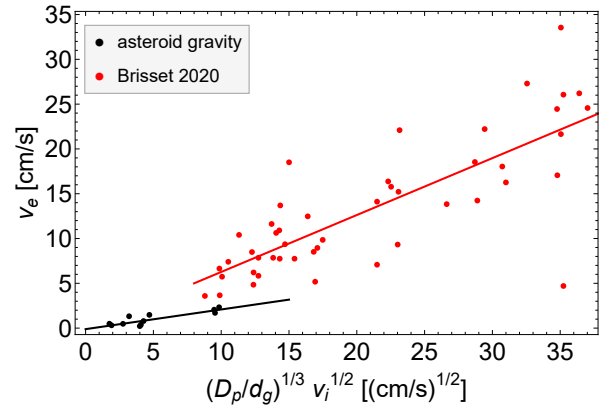


FIG. 6: Low gravity experimental data compared in detail. Red: Brisset 2020. Black: Asteroid gravity  $2 \cdot 10^{-3} \text{ m/s}^2$

periment, the scaling is not universal for all gravity regimes, the linear fits do not match. Additional parameters might be necessary to collapse the data onto each others. Under earth gravity, no observable ejecta are produced for impactor velocities of  $120 \text{ cm/s}$  or lower. Fits to the simulated data follow a clear trend with respect to the ambient gravity. As displayed in Fig. 7, the slope increases with gravity. This in turn gives reason to compare slopes of the two subsets of reduced gravity data, as shown in 6. The individual fit to our data set yields a  $m_l = 0.22$ , while the fit to the literature values yields a  $m_l = 0.635$ . Compared to numerical values those values can be attributed to simulated environmental accelerations. The value for  $m_a$  lies between the slopes for  $0.002 \text{ m/s}^2$  and  $0.01 \text{ m/s}^2$  with  $m_{0.002} = 0.178$  and  $m_{0.01} = 0.247$ , while  $m_l$  lies close  $m_{0.5} = 0.666$  and  $m_1 = 0.694$ , within the uncertainties of those fit parameters. The vertical range of the red red area in Fig. 7 denotes the gravity range of  $10^{-4} \text{ g}$  to  $10^{-2} \text{ g}$ <sup>18</sup>.

### III. DISCUSSION

Our experiment extends the previously known velocity distribution of ejecta to even lower impact velocity. This extension allows to test the ejecta velocity scaling found by Brisset *et al*. We show, that the linear trend in Fig. 3 for ejecta velocities extends into the regime of extremely slow impacts at low partial gravity. This trend is not observed at earth gravity. While the experimental earth gravity data comes with a higher uncertainty, it is set apart from the low gravity results in a similar way in our simulations. We now argue, that one reason for why the Earth gravity data does not fit into this scaling is due to the fact that gravity sets a lower limit for observable ejecta velocities, thus in turn shifting observed mean velocities towards higher values. Since this cutoff is also applied to the simulation data, the observed similarity supports this hypothesis. Comparing the scaled experimental data from our experiments to the experiments featured in Brisset *et al*.<sup>8</sup> (Fig.6), we notice a difference if we fit the linear model to the data sets individually. Trying to explain this, we show the slopes of those models in Fig. 7 together with the slopes obtained

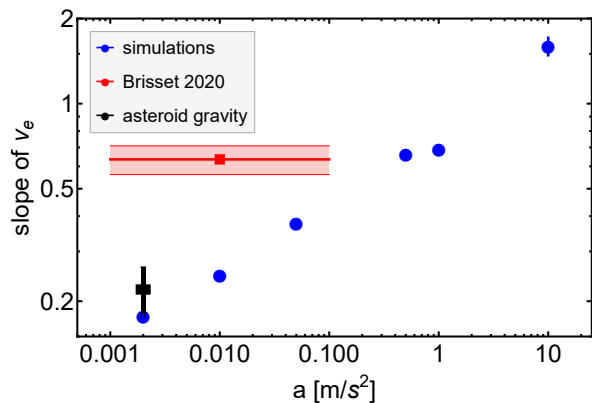


FIG. 7: Slopes of linear fits from 4. Blue: Simulations. Red: Data from Brisset 2020<sup>8</sup>. Black: Data from our experiment. Uncertainties from standard error of fit parameters. The vertical scale of the red area denotes the range of accelerations given in Brisset *et al.*<sup>18</sup>.

from simulation data at different gravity levels. We also indicate the range of gravities under which the experiments were performed. Our data agrees with the simulation data within margin of error. For the literature data, our simulation data does not agree as well but would suggest either a higher gravity level, a different observed velocity cutoff or observation time.

## IV. METHODS

### A. Experiment Methods

This section gives a short overview of the experiment. For details and performance evaluation of the experimental setup and carrier platform see Joeris, Keulen, and Kollmer<sup>17,16,20</sup>. The core idea is the accurate recreation of asteroid conditions in a controlled environment. To fulfill those requirements, we conduct our experiment at the ZARM drop tower in Bremen. The overall structure of the experiment is as follows: In the evacuated drop tower, a pressurized capsule is launched vertically by a catapult. The capsule is then in free flight and thus experiencing zero gravity. The drop tower guarantees a very clean microgravity with residual accelerations of  $10^{-6} \text{ m/s}^2$  for  $9.2 \text{ s}$ <sup>21</sup>. Inside the free falling drop tower capsule, our vacuum chamber is attached to a linear stage. This linear stage drives with a constant acceleration of  $a_a = 2 \cdot 10^{-3} \text{ m/s}^2$ , creating a controlled asteroid gravity environment. Inside of the experiment vacuum chamber, a launcher is located, which is able to haul impactors onto the asteroid simulat surface at the bottom of the chamber. Each impactor is a irregularly shaped basaltic particle with a diameter of  $\approx 3 \text{ mm}$ . The whole scene is observed with cameras from three different angles. The main camera observes the front of the chamber, perpendicular to the impactor's line of flight and slightly angled to the granular bed's surface. For a view from the main camera, see Fig. 1. The left panel, Fig. 1a shows an example impact with

some highlighted main components. It is a combination of two images from different time points, split by a horizontal white line. The top part, marked **i**, shows the launcher assembly right after the launch. The impactor, marked with a red circle, is being pushed out of its compartment by a rod moved by a solenoid. While the impactor is retained until shortly before its launch, in the depicted situation the hatch used to retain the impactor is moved out of its way and positioned behind the solenoid rod and the impactor, itself marked with a white outline. The lower part of the image shows a later time frame, marked with a white **ii**. Clearly visible is the rebounding impactor, again marked with a red circle. Its trajectory is marked with a dashed red line. Around the site of the impact, a plume of ejecta can be observed. To make the ejecta plume's development more clear, Fig. 1b is included. Here, we show an automated tracking performed on a binarized image sequence. The trajectory of each particle is shown in blue, with the length hinting on its velocity and the particle itself marked in red. Limitations of this method are already apparent: Many particles are wrongly detected and deviations from the actual smooth trajectory yield a systematic overestimation of velocities for this particle size. Other methods for ejecta characterization are detailed below.

### 1. Particle Velocity Determination

The impactor's velocity is measured manually in all cases, by tracking it using the main camera. The ejecta velocities are measured using the main camera located at the chamber's front, with optical axis near perpendicular to the impactor's flight direction and the simulat surfaces normal vector. From the image data obtained with this setup, the velocities are extracted using three different methods.

The simplest one is the direct tracking method. Here, particles are located individually using footage from the main camera and identified individually and manually over as many frames as possible. This method only works for targets composed of larger grains and ejecta populations which consist of only a few grains. For those cases of course it becomes most reliable and accurate and can provide a benchmark for the accuracy of other velocity field measurement methods. The error of this method is determined by spatial and temporal resolution. With an increasing number this method becomes less feasible. Still, with ejecta numbers below 30, a different variant of this method can be used, but the number of observed frames has to be decreased. Here, the velocity is determined from only two frames and averaged over all particles. As a third variant, useful for small particles, what we call the radius method is employed. Here, a half circle is positioned around the impact point. Then the time is measured from impact until the ejecta passes the half circle. For each impact, this was done using each three radii.

Automated tracking does not work well for our irregular, low contrast particles. An example image with many incorrectly identified particles is shown in Fig. 1b. But while

individual particles cannot be resolved reliably, the flow field yields information. So, in cases with strong ejecta production and small bed particles, particle imaging velocimetry (PIV) is used. PIV is a technique widely used in fluid dynamics, usually employed to examine flows of fluids or gasses. Images of tracer particles inserted into the examined flowing medium are taken at two time points. The image is then partitioned into interrogation regions and both images cross-correlated, to find a two dimensional flow vector. Applying the technique to our data is straight-forward: An image pair is composed of two consecutive images from our video data. We do not examine a flowing medium, but are interested in the particles themselves. Specifically, we use the PIV plugin distributed with the open source image processing package **Fiji**. The time interval in which the splash occurs is isolated and the frame rate reduced to leave 20 frames. PIV is performed for each two consecutive images. The interrogation window is chosen to 1/8 of the original image dimension, with the search window double its size and the vector spacing half its size. The next interrogation window sizes are reduced by a factor of 1/2 for each iteration. For further investigation the third iteration is used.

## B. Simulation Methods

The physical system was additionally recreated in a numerical simulation. We used the LIGGGHTS software package<sup>22</sup>, an open source project for discrete-element methods. Grains are modeled as spherical particles. In the simulation, the experiment was recreated. To achieve this, a set of 32891 spherical particles with diameters of 0.9 mm radius is dropped into a cylindrical container with a diameter of 10 cm and a depth of 2 cm. Settling of the granular bed is performed a gravity of  $10 \text{ m/s}^2$ , close to earth gravity, to better resemble the experiment. Before insertion of the impactor, the gravity is reduced to the targeted gravity of  $a_a = 2 \cdot 10^{-3} \text{ m/s}^2$  or kept at  $10 \text{ m/s}^2$  for earth gravity control measurements. After settling, an impactor is inserted above the granular bed's surface with a given initial velocity with only one non vanishing component parallel to the gravity vector, essentially launching it in the direction of the granular bed. For the contact model a dissipative Hertzian model was chosen (gran model hertz in LIGGGHTS) with a linearized variant of Johnson-Kendall-Roberts<sup>23</sup> cohesion (SKJR2). Further simulation parameters chosen are the following: Particle density was set to  $2.1 \text{ g/cm}^3$ , which is in the range of the bulk density of silicates like soda lime glass or basalt<sup>24,25</sup>, while allowing some additional porosity. The Young's modulus is set to  $10^9 \text{ Pa}$ , which is about one to two orders of magnitude lower than that of real basalt<sup>26</sup> to allow for smaller simulation time steps and a shorter simulation time. The Poisson ratio is set to 0.2, the coefficient of friction to 0.2, the coefficient of restitution to 0.5 and the cohesion energy density to  $21600 \text{ ergs/cm}^3$ .

## V. AUTHOR DECLARATIONS

### A. Conflict of Interests

The authors have no conflicts to disclose.

### B. Acknowledgements

This work was supported by the DLR Space Administration with funds provided by the Federal Ministry for Economic Affairs and Climate Action (BMWK) based on a decision of the German Federal Parliament under grant number 50WM1943, 50WK2270C and 50WM2243.

### C. Author Contributions

**Kolja Joeris:** Investigation (lead); Resources (lead); Software (lead); Writing - original draft (lead); Visualization (lead); **Laurent Schönau:** Investigation (supporting); ; Writing - original draft (supporting); Visualization (supporting). **Matthias Keulen:** Investigation (supporting); Writing - original draft (supporting); Visualization (supporting). **Jonathan E. Kollmer:** Conceptualization (lead); Supervision (lead) Project Administration (lead); Funding Acquisition (lead); Writing - original draft (supporting).

<sup>1</sup>H. Yano, T. Kubota, H. Miyamoto, T. Okada, D. Scheeres, Y. Takagi, K. Yoshida, M. Abe, S. Abe, O. Barnouin-Jha, *et al.*, "Touchdown of the hayabusa spacecraft at the muses sea on itokawa," *Science* **312**, 1350–1353 (2006).

<sup>2</sup>D. S. Lauretta, H. L. Enos, A. T. Polit, H. L. Roper, and C. W. Wolner, "Osiris-*rex* at bennu: Overcoming challenges to collect a sample of the early solar system," in *Sample return missions* (Elsevier, 2021) pp. 163–194.

<sup>3</sup>M. Arakawa, T. Saiki, K. Wada, K. Ogawa, T. Kadono, K. Shirai, H. Sawada, K. Ishibashi, R. Honda, N. Sakatani, *et al.*, "An artificial impact on the asteroid (162173) ryugu formed a crater in the gravity-dominated regime," *Science* **368**, 67–71 (2020).

<sup>4</sup>J.-Y. Li, M. Hirabayashi, T. L. Farnham, J. M. Sunshine, M. M. Knight, G. Tancredi, F. Moreno, B. Murphy, C. Opitom, S. Chesley, *et al.*, "Ejecta from the dart-produced active asteroid dimorphos," *Nature* **616**, 452–456 (2023).

<sup>5</sup>A. F. Cheng, H. F. Agrusa, B. W. Barbee, A. J. Meyer, T. L. Farnham, S. D. Raducan, D. C. Richardson, E. Dotto, A. Zinzi, V. Della Corte, *et al.*, "Momentum transfer from the dart mission kinetic impact on asteroid dimorphos," *Nature* **616**, 457–460 (2023).

<sup>6</sup>T. Bogdan, J. E. Kollmer, J. Teiser, M. Kruss, and G. Wurm, "Laboratory impact splash experiments to simulate asteroid surfaces," *Icarus* **341** (2020).

<sup>7</sup>J. E. Colwell, S. Sture, M. Cintala, D. Durda, A. Hendrix, T. Goudie, D. Curtis, D. J. Ashcom, M. Kanter, T. Keohane, *et al.*, "Ejecta from impacts at 0.2–2.3 m/s in low gravity," *Icarus* **195**, 908–917 (2008).

<sup>8</sup>J. Brisset, C. Cox, S. Anderson, J. Hatchitt, A. Madison, M. Mendonca, A. Partida, and D. Remie, "Regolith behavior under asteroid-level gravity conditions: Low-velocity impacts into mm- and cm-sized grain targets," *Astron. Astrophys* (2020), 10.1051/0004-6361/202038665.

<sup>9</sup>C. Sunday, N. Murdoch, O. Cherrier, S. Morales Serrano, C. Valeria Nardi, T. Janin, I. Avila Martinez, Y. Gourinat, and D. Mimoun, "A novel facility for reduced-gravity testing: A setup for studying low-velocity collisions into granular surfaces," *Review of Scientific Instruments* **87** (2016).

<sup>10</sup>N. Murdoch, P. Sánchez, S. R. Schwartz, and H. Miyamoto, "Asteroid surface geophysics," arXiv preprint arXiv:1503.01931 (2015).

- <sup>11</sup>K. J. Walsh, “Rubble pile asteroids,” *Annu. Rev. Astron. Astr.* **56**, 593–624 (2018).
- <sup>12</sup>A. Fujiwara, J. Kawaguchi, D. K. Yeomans, M. Abe, T. Mukai, T. Okada, J. Saito, H. Yano, M. Yoshikawa, D. J. Scheeres, O. Barnouin-Jha, A. F. Cheng, H. Demura, R. W. Gaskell, N. Hirata, H. Ikeda, T. Kominato, H. Miyamoto, A. M. Nakamura, R. Nakamura, S. Sasaki, and K. Uesugi, “The rubble-pile asteroid Itokawa as observed by Hayabusa,” *Science* **312**, 1330 (2006).
- <sup>13</sup>H. Miyamoto, H. Yano, D. J. Scheeres, S. Abe, O. Barnouin-Jha, A. F. Cheng, H. Demura, R. W. Gaskell, N. Hirata, M. Ishiguro, *et al.*, “Regolith migration and sorting on asteroid itokawa,” *Science* **316**, 1011–1014 (2007).
- <sup>14</sup>Y. Jiang and J. Schmidt, “Motion of dust ejected from the surface of asteroid (101955) bennu,” *Heliyon* **6** (2020).
- <sup>15</sup>D. J. Scheeres, C. M. Hartzell, P. Sánchez, and M. Swift, “Scaling forces to asteroid surfaces: The role of cohesion,” *Icarus* **210**, 968–984 (2010).
- <sup>16</sup>K. Joeris, L. Schönau, M. Keulen, P. Born, and J. E. Kollmer, “The influence of interparticle cohesion on rebounding slow impacts on rubble pile asteroids,” *npj Microgravity* **8**, 36 (2022).
- <sup>17</sup>K. Joeris, M. Keulen, and J. E. Kollmer, “Controlled partial gravity platform for milligravity in drop tower experiments,” (2024), arXiv:2411.12391 [astro-ph.IM].
- <sup>18</sup>J. Brisset, J. Colwell, A. Dove, S. Abukhalil, C. Cox, and N. Mohammed, “Regolith behavior under asteroid-level gravity conditions: low-velocity impact experiments,” *Progress in Earth and Planetary Science; Heidelberg* **5**, 1–21 (2018).
- <sup>19</sup>J. E. Colwell, “Low velocity impacts into dust: results from the collide-2 microgravity experiment,” *Icarus* **164**, 188–196 (2003).
- <sup>20</sup>K. Joeris, L. Schönau, L. Schmidt, M. Keulen, V. Desai, P. Born, and J. Kollmer, “Experiments on rebounding slow impacts under asteroid conditions,” *EPJ Web of Conferences* **249**, 13003 (2021).
- <sup>21</sup>P. Von Kampen, U. Kaczmarczik, and H. J. Rath, “The new drop tower catapult system,” *Acta Astronautica* **59**, 278–283 (2006).
- <sup>22</sup>C. Kloss, C. Goniva, A. Hager, S. Amberger, and S. Pirker, “Models, algorithms and validation for opensource dem and cfd-dem,” *Prog. Comput. Fluid. Dy.* **12**, 140–152 (2012).
- <sup>23</sup>K. Johnson, K. Kendall, and A. Roberts, “SURFACE ENERGY AND CONTACT OF ELASTIC SOLIDS,” *Proc. R. Soc. Lon. Mat.* **324**, 301 (1971).
- <sup>24</sup>T. Steinpilz, K. Joeris, F. Jungmann, D. Wolf, L. Brendel, J. Teiser, T. Shinbrot, and G. Wurm, “Electrical charging overcomes the bouncing barrier in planet formation,” *Nat. Phys.* **16**, 225+ (2020).
- <sup>25</sup>M. Le Bas and A. L. Streckeisen, “The iugs systematics of igneous rocks,” *Journal of the Geological Society* **148**, 825–833 (1991).
- <sup>26</sup>C. E. Vennari, F. Lin, M. Kunz, M. Akaogi, L. Miyagi, and Q. Williams, “Deformation and strength of mantle relevant garnets: Implications for the subduction of basaltic-rich crust,” *American Mineralogist* **106**, 1045–1052 (2021).